Journal of Microscopy, Vol. 228, Pt 1 2007, pp. 97–102
Received 29 June 2006; accepted 11 April 2007

Specimen-induced distortions in light microscopy

M. SCHWERTNER*, M. J. BOOTH & T. WILSON
Department of Engineering Science, University of Oxford, Parks Road, Oxford OX1 3PJ, U.K.

Key words. Confocal microscopy, measurement accuracy, multiphoton microscopy, spatial distortions, specimen-induced aberrations.

Summary

Specimen-induced aberrations affect the imaging properties in optical 3D microscopy, especially when high numerical aperture lenses are used. Studies on aberrations are often properly concerned with the degradation of image quality such as compromised resolution or reduced signal intensity. Apart from these, aberration effects can also introduce geometric image distortions. The effects, discussed here are particularly strong when thick biological specimens are investigated. Using a high numerical aperture interferometer, we measured wavefront aberrations in transmission mode and quantified geometric distortions associated with specimen-induced aberrations. This assessment for a range of biological specimens allows estimation of the accuracy of spatial measurements. The results show that high-resolution spatial measurements can be significantly compromised by specimen-induced aberrations.

Introduction

In an ideal microscope, spherical wavefronts converge towards an optimum, diffraction limited focal spot at the nominal focal position (NFP). Unfortunately and inevitably, the specimen under examination can introduce deviations from this ideal wavefront which lead to an aberrated focal spot. The effect of these aberrations can be divided into two broad classes. The first type of aberrations produces a blurred and enlarged focal spot which leads to a loss in resolution and image intensity. This effect has been the subject of many studies and its correction is the goal of adaptive optics. In this article, we are concerned with the second effect of aberrations which has little or minimal influence on the intensity distribution of the focal spot but creates displacement between then actual focal position (AFP) and the NFP as illustrated in Fig. 1. It should be pointed out that this effect is typically small for commonly used biological preparations in the form of very thin sections or individual cells. However, it can be significant for thick biological specimens.

A standard 3D microscope system maps the intensity sampled at the AFP into a 3D dataset using the NFP information. This can lead to strong spatial distortions, as illustrated in (Pawley, 2002), and may also lead to measurement inaccuracies. The effect of specimen-induced spherical aberration and the resulting discrepancy between NFP and AFP due to refractive index mismatch has been investigated already (Hell *et al.*, 1993).

In the standard epi configuration that is common in fluorescence microscopy, the lateral displacement cannot be inferred from the wavefront that is originating from the focal spot because of the reciprocal geometry. Therefore, in order to measure the distortion introduced by a number of specimens, we employed the single pass transmission geometry shown on the right of Fig. 1 together with an interferometer to measure the wavefront in the pupil plane of the lens.

Experimental set-up

We built a Mach-Zehnder phase stepping interferometer to measure the aberrations induced by various biological specimens in transmission geometry. The specimen was placed in the object path between two opposing 1.2 NA water immersion lenses. A phase stepping unit was located in the reference beam path and took the form of a flat mirror mounted on a calibrated piezo drive. More details on the experimental set-up can be found in (Schwertner *et al.*, 2004b). Our interferometer measures aberrations in transmission including the path beyond the focal spot. Therefore, one has to be aware that the aberrations measured are strictly equivalent to the epi case only when the focus is set to be beyond the specimen such that the light traverses the entire specimen on the way from the lens to the focal spot. Then no further aberrations are introduced beyond the focal spot. This limitation is not severe since the strongest aberrations may occur when the whole specimen is traversed. For all of our measurements, the focus was set to the bottom of

*New address: Carl Zeiss MicroImaging GmbH, Carl Zeiss Group, Carl Zeiss Promenade 10, 07745 Jena, Germany. Correspondence to: T. Wilson. e-mail: Tony.Wilson@eng.ox.ac.uk

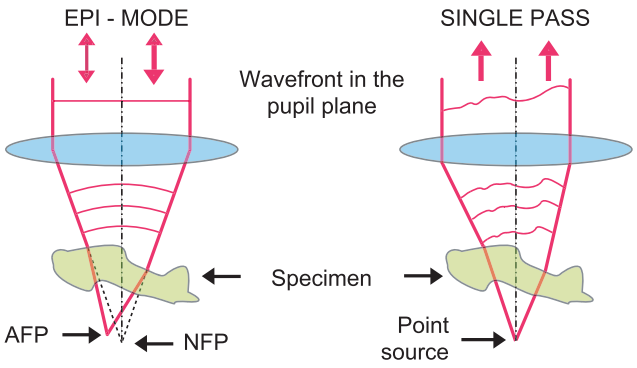

Fig. 1. Left: Specimen-induced aberrations and their effect in epi configuration. Because of the variation in refractive index within the specimen, the actual focal position (AFP) of the focal spot can be different from the nominal focal position (NFP). Right: Wavefront aberrations can be measured in the pupil plane of the lens in a single pass configuration when a point source is placed in the nominal focal spot position. The measured wavefront information allows to model the position and shape of the focal spot in the equivalent epi configuration.

the specimen in order to determine the maximum effect of specimen-induced distortion so as to establish estimates for the spatial measurement accuracy.

Data acquisition and analysis

As detailed in Schwertner *et al.* (2004a,2004b), the Mach-Zehnder interferometer uses phase stepping and allows to measure the phase function $\Psi(\xi, \eta)$ within the pupil plane of the lens. For each specimen, 256 wavefronts are recorded on a 16 × 16 grid. The wavefront aberrations can then be described by the complex pupil function

$$P(\xi, \eta) = \exp[j\Psi(\xi, \eta)], \tag{1}$$

where $j = \sqrt{-1}$, the Cartesian coordinates (ξ, η) refer to the pupil plane of the lens, the pupil plane radius is normalized to unity and we assumed uniform amplitude. The phase function can also be represented by a series of Zernike polynomials:

$$\Psi(\xi, \eta) = \sum_{i=1}^{N} M_i \, Z_i(\xi, \eta), \tag{2}$$

where Z_i is the Zernike polynomial with index i and M_i the corresponding mode amplitude. Knowledge of the phase function allows us to extract the mode coefficients, as we have done in Schwertner *et al.* (2004a,b). Some of these coefficients correspond to classical aberration terms, such as coma, astigmatism or spherical aberration, and effect imaging quality. However, here we concentrate on the three lower-order Zernike terms: tip, tilt and defocus corresponding to the Zernike coefficients M_2, M_3 and M_4, respectively. They are not considered aberrations in the classical sense but they represent geometrical distortion of the image, a deviation of the actual position of the focal spot from its nominal position.

To relate the measured Zernike coefficients to displacements in the focal region, we consider the intensity distribution at the focus (Wilson and Sheppard, 1984):

$$I(t, w, u) = \left| \int_0^{2\pi} \int_0^1 P(\xi, \eta) \exp\left[j\frac{u}{2}(\xi^2 + \eta^2) - j(\xi t + \eta w) \right] \mathrm{d}\xi \, \mathrm{d}\eta \right|^2 . \tag{3}$$

Here we have used the normalized optical coordinates:

$$u = \frac{8\pi}{\lambda} n z \sin^2(\alpha/2) \tag{4}$$

in the axial direction and

$$t = \frac{2\pi}{\lambda} x \, n \sin\alpha \quad ; \quad w = \frac{2\pi}{\lambda} y \, n \sin\alpha \tag{5}$$

in the lateral direction. The term $n \sin\alpha$ refers to the numerical aperture (NA) and λ is the wavelength. The variables x, y and z denote the actual radial and axial coordinates in the focal region. Now we consider a specific pupil function containing only the Zernike terms corresponding to tip, tilt and defocus:

$$P(\xi, \eta) = \exp\left[j \left(M_2 Z_2(\xi, \eta) + M_3 Z_3(\xi, \eta) + M_4 Z_4(\xi, \eta) \right) \right]. \tag{6}$$

Here the corresponding Zernike polynomials in Cartesian coordinates are defined as (Noll, 1976)

$$Z_2 = 2\xi; \quad Z_3 = 2\eta \quad \text{and} \quad Z_4 = \sqrt{3}(2(\xi^2 + \eta^2) - 1). \tag{7}$$

When we introduce (6) into Eq. (3) and compare the coefficients in the arguments of the exponentials, we find that the effects of the aberration modes (7) is to introduce a shift, Δ, in the x, y and z directions given by

$$\Delta x = \frac{M_2 \lambda}{\pi n \sin\alpha}; \quad \Delta y = \frac{M_3 \lambda}{\pi n \sin\alpha}; \quad \Delta z = -\frac{M_4 \sqrt{3} \lambda}{2\pi n \sin^2(\alpha/2)}. \tag{8}$$

The above expressions allow us to calculate the displacement of the focal spot directly from the Zernike mode coefficients for tip, tilt and defocus extracted from $\Psi(\xi, \eta)$.

The calculation based on Eq. (3) is an approximation that is valid for relatively small variations in refractive index only. We also note that, for high NA lenses, defocus is represented by a pupil function consisting of even order polynomials including terms in ρ^4 and higher orders. In our expression (3), we have approximated defocus by the dominant quadratic term.

Results and discussion

In order to quantify the specimen-induced distortions, we processed wavefront data from a variety of biological specimens; the characteristics are listed in Table 1. We chose examples that represent common specimen categories. For confocal or multiphoton techniques, high NA lenses are

Table 1. Specimen list (PBS: phosphate buffered saline).

Specimen no.	Description	Embedding	Thickness [μm]	Lateral scan [μm]
1	Brain tissue, rat	PBS	30	120 × 120
2	Mouse oocyte	PBS	80	125 × 125
3	Liver tissue, mouse	PBS	20	20 × 20
4	Striated muscle, rat	PBS	40	50 × 50
5	C. elegans	Agar gel	40	50 × 50
6	Vas deferens, rat	PBS	30	50 × 50

usually preferred because of their superior light collection efficiency and resolution. However, some applications can require lower NA lenses and therefore we investigated the effect of specimen-induced distortions at lower NA as well. In both cases, the wavefront information was extracted from the datasets recorded with a 1.2 NA water immersion lens. For the lower NA, a smaller circular subregion of the interferograms corresponding to a NA of 0.6 was analyzed and Zernike modes were fitted to this subregion using the same procedure.

The local displacements of the focal spot calculated using the method above are displayed in Fig. 2 for the NA of 1.2 and in Fig. 3 at the lower NA of 0.6. For each specimen, the deviations in the x, y and z directions are shown separately. The measured distortions correlate well with the geometry of the specimens. The field of view for the measurement of specimen 1, for example, includes a horizontal edge of the tissue. This can be clearly identified in the Y-components of the distortion for specimen 1.

Statistical data on the distortion, such as the individual standard deviations in the X,Y and Z directions are listed in Table 2 and the maximum value of the total spatial deviation $d = \sqrt{\Delta x^2 + \Delta y^2 + \Delta z^2}$ for each specimen is also given.

The total 3D displacement of the spot, depending on specimen structure and location within the specimen, can exceed 1 μm. The patterns observed correlate with the specimen structures as expected. For example, the scan of specimen no. 1 contains the horizontal edge of the tissue, which causes distortion in the y and z directions but leaves the x-component almost unaffected. The largest distortion value in the order of 2 μ m was found within a particular region of the mouse oocyte cell (specimen no. 2) at an NA of 0.6, where the axial component was dominant.

To understand the influence of the NA on the specimen-induced distortions, we turn to the illustrations of Fig. 4. Here, cross-sections $\Psi(r)$ of two-dimensional phase functions $\Psi(r, \theta)$ in the pupil plane of the lens are shown for three different situations. Using a lens of larger NA is equivalent to capturing a larger range of the same wavefront or phase function. In Fig.(a), the simplest case is depicted where the phase function is a constant slope function. Then the average wavefront tilt across

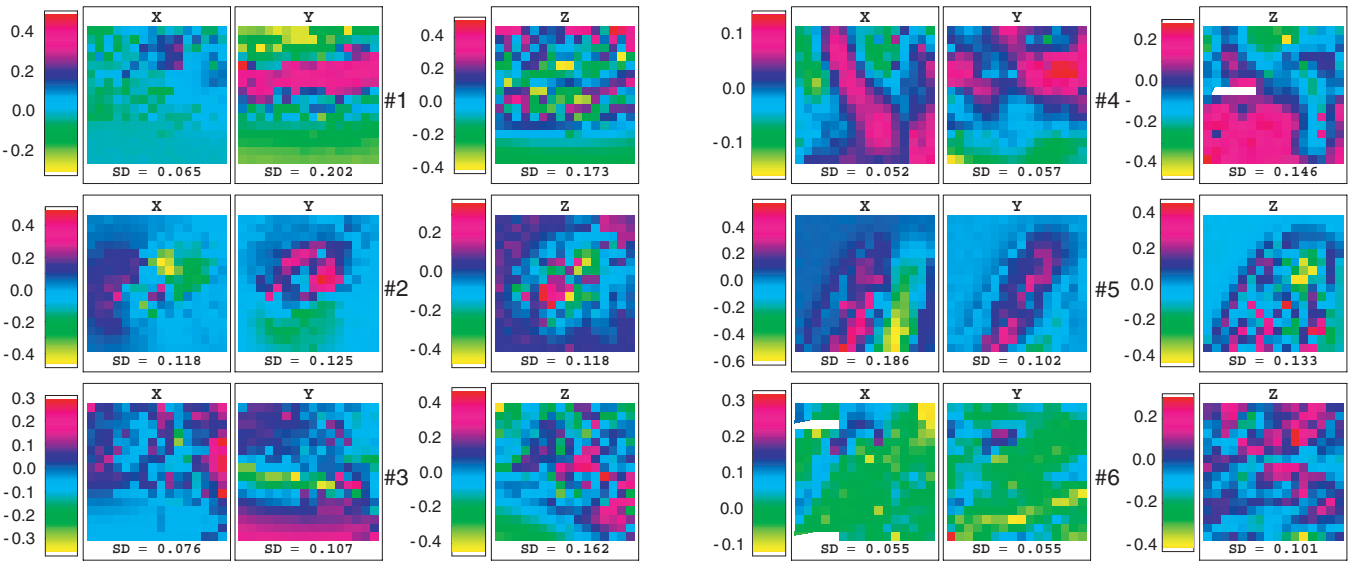

Fig. 2. Specimen-induced distortion at an NA of 1.2. The specimen numbers 1 to 6 refer to the description in Table 1. The abbreviation SD denotes the standard deviation of the distortion calculated across the field of view. Units are micrometers.

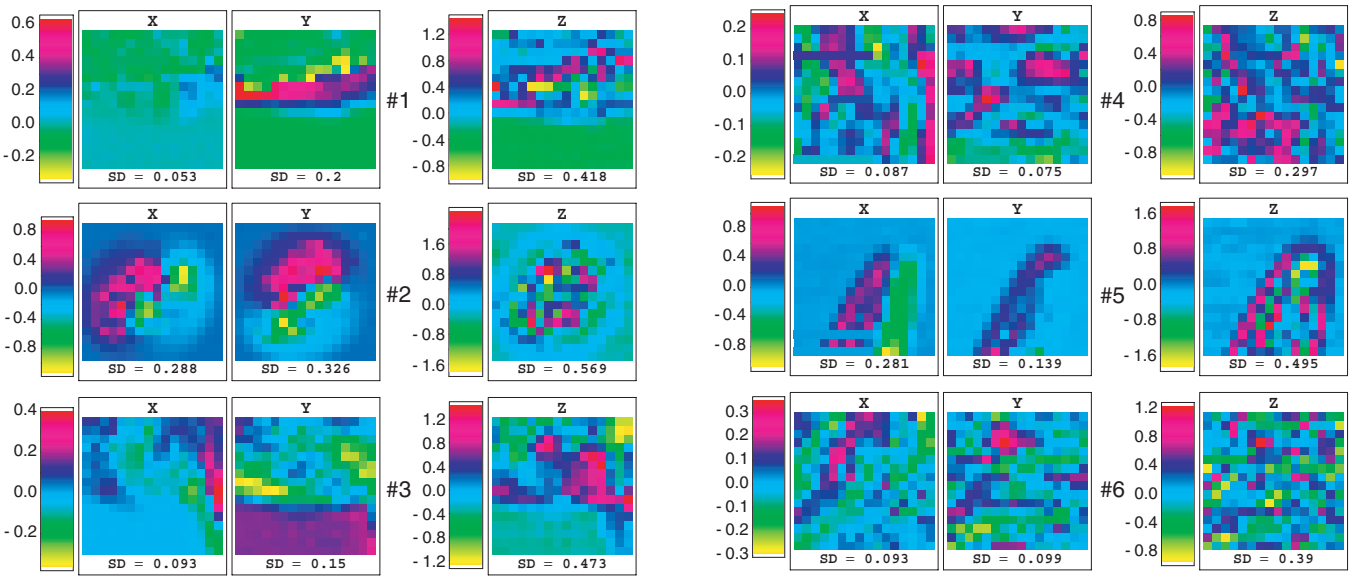

Fig. 3. Specimen-induced distortion at an NA of 0.6. The specimen numbers 1 to 6 refer to the description in Table 1. The abbreviation SD denotes the standard deviation of the distortion calculated across the field of view. Units are micrometers.

Table 2. Statistical properties of the measured specimen-induced focal spot displacements. Units are micrometers.

Specimen no.	NA	StdDev(X)	StdDev(Y)	StdDev(Z)	MaxDev(total)
1	1.2	0.065	0.202	0.173	0.521
	0.6	0.053	0.200	0.418	1.563
2	1.2	0.118	0.125	0.118	0.672
	0.6	0.288	0.326	0.569	2.080
3	1.2	0.076	0.107	0.162	0.491
	0.6	0.093	0.150	0.473	1.440
4	1.2	0.052	0.057	0.146	0.457
	0.6	0.087	0.075	0.297	1.090
5	1.2	0.186	0.102	0.133	0.713
	0.6	0.281	0.139	0.495	1.911
6	1.2	0.076	0.107	0.162	0.423
	0.6	0.093	0.099	0.390	1.270

the pupil is the same for the lower NA of 0.6 and the higher NA of 1.2 and focal spot displacements are identical for both NAs[1]. However, typical aberration patterns tend to be more complicated, which can lead to a dependence of the specimen-induced distortion on the NA. In part (b) of Fig. 4, such an example is illustrated for lateral distortion: The same phase function leads to different average wavefront slopes across the pupil for different NAs. A similar situation is illustrated in Fig. 4(c), for axial specimen induced distortion. The source of axial distortion is a quadratic term in the phase function (defocus). From Fig. 4(c), you can read that the displayed phase function has a dominant first-order spherical aberration term at the higher NA of 1.2, although the quadratic term, indicating axial displacement, is only minor. This is exactly opposite at lower NA, where the axial displacement (quadratic component) dominates, although the spherical aberration component is very small. This example also coincides with the general observation that larger NAs lead to higher spatial frequencies in the aberration function and therefore require higher aberration orders for the appropriate description and/or correction.

Another representation of the results for an NA of 0.6 is also shown in Fig. 5. Here the imaging of a regular square grid underneath the specimen is simulated and the mesh-knots of the regular grid are displaced according to the measured deviations. Note that the effect is exaggerated in the drawing - the mesh-knot displacement is drawn five times larger at the scale of the grid.

When a relative measurement within a 3D dataset is done, both the absolute errors of the two individual spot position measurements contribute to the inaccuracy of the relative position measurement. In the worst case, the individual distortions will add up. The data imply that the effect of specimen-induced aberrations can easily lead to a distance measurement inaccuracy in the order of 1 μm to 2 μm. Considering that typical cell dimensions are in the range from 5 to 20 μm, this can lead to large relative errors. If, for example, a distance of approximately 5 μm has to be measured within a cell and the uncertainty of the distance measurement is 1 μm, the expected relative error is 20 % and hence these effects cannot be neglected.

[1] Note that the Zernike mode coefficients are calculated for a pupil normalized to unity. Therefore, the NA of 1.2 would yield twice the tip/tilt Zernike coefficients compared to the NA of 0.6 but this is compensated for by the NA-dependence of the conversion between Zernike mode units and spot displacement/distortion (see Eq. 8).

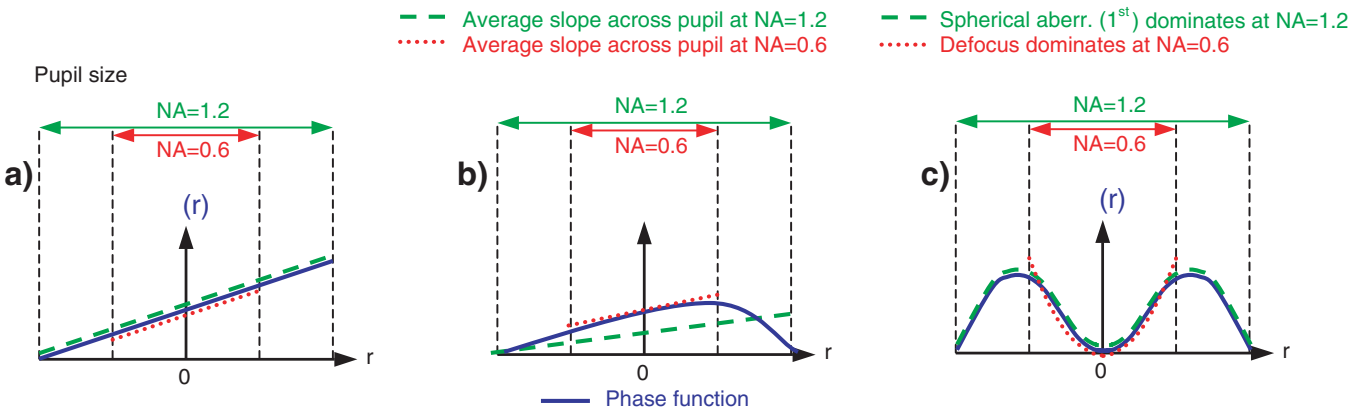

Fig. 4. Illustration on the dependence on the specimen-induced distortions and other aberrations on the numerical aperture (NA). Please see text.

Conclusion

We have presented a method to obtain quantitative data for the spatial measurement inaccuracies due to specimen-induced aberrations. The approach uses interferometry to record wavefront aberration data from the pupil plane of the microscope lens to extract information about local distortion. To our knowledge, this is the first attempt to quantify the effects of specimen-induced image distortion in microscopy. Our results show that that specimen-induced distortions can significantly influence the spatial measurement accuracy that can be achieved with an otherwise perfect and calibrated microscope.

Correction of the distortion effects discussed is possible but seems challenging in practical microscope systems. If the wavefront aberrations are known, one could use these data for a software correction of the geometrical distortions. However, direct measurement of the required tip, tilt and defocus components of the wavefront is not possible in the most common epi illumination configuration due to its reciprocal optical path. The distortion could be determined if one could obtain the refractive index profile of the specimen. This might be found indirectly, for example, through tomography based upon phase measurements within an adaptive optical microscope (Booth *et al.*, 2002) or a digital holographic microscope (Montfort *et al.*, 2006).

Acknowledgements

M.S. is supported by the DAAD Germany (German Academic Exchange Service). M.J.B. is a Royal Academy of Engineering/EPSRC Research Fellow. We would like to thank the following for providing specimens: Richard Gardner and Tim Davis, Department of Zoology, Oxford; Allison Woollard, Department of Biochemistry, Oxford; Tom Cunnane, Keith Brain and Patricia Tynan, Department of Pharmacology,

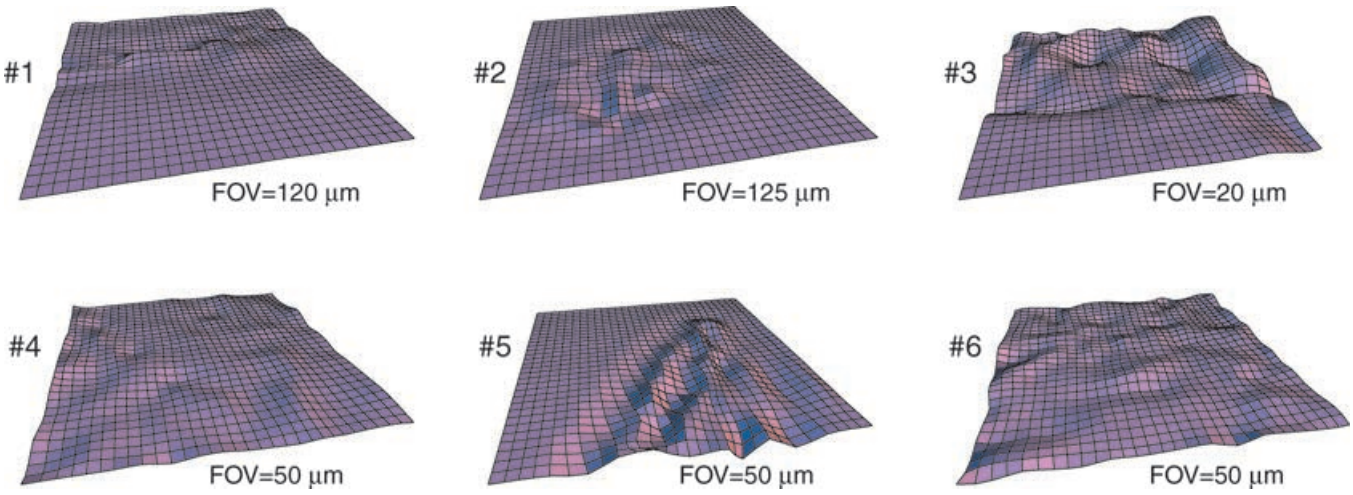

Fig. 5. Visualization of the specimen-induced distortions at an NA of 0.6: simulation of imaging a regular grid placed underneath the specimen. The measured distortions are plotted as a deviation from the regular mesh positions of the grid and are enlarged by a factor of 5. The specimen numbers refer to Table 1 and the field of view (FOV) covered by the scan is also given for each specimen.

Oxford. This work was supported by Carl Zeiss Jena GmbH and Research Councils U.K. under the Basic Technology scheme.

References

Booth, M.J., Neil, M.A.A., Juškaitis, R. & Wilson, T. (2002) Adaptive aberration correction in a confocal microscope. *Proc. Nati. Acad. Sci. USA* **99**, 5788–5792.

Hell, S., Reiner, G., Cremer, C. & Stelzer, E.H.K. (1993) Aberrations in confocal fluorescence microscopy induced by mismatches in refractive index. *J. Microsc.* **169**, 391–405.

Montfort, F., Colomb, T. Charriere, F., Kuehn, J., Marquet, P., Cuche, E., Hermingard S. & Depeursinge C. (2006) Submicrometer optical tomography by multiple-wavelength digital holographic microscopy. *Appl. Opt.* **45**, 8209–8217.

Noll, R.J. (1976) Zernike polynomials and atmospheric turbulence. *J. Opt. Soc. Am.* **66**, 207–277.

Pawley, J.B. (2002) Limitations on optical sectioning in live-cell confocal microscopy. *Scanning* **24**, 241–246.

Schwertner, M., Booth, M.J., Neil, M.A.A. & Wilson, T. (2004a) Measurement of specimen-induced aberrations of biological samples using phase stepping interferometry. *J. Microsc.* **213**, 11–19.

Schwertner, M., Booth, M.J. & Wilson, T. (2004b) Characterizing specimen induced aberrations for high na adaptive optical microscopy. *Opt. Express* **12**, 6540–6552.

Wilson, T. & Sheppard, C.J.R. (1984) *Theory and Practice of Zcanning Optical Microscopy*, Academic Press, London.

